



HAL
open science

Use of external magnetic field for supervision and diagnosis of electrical traction motors

Remus Pusca, Raphael Romary, Adrian Ceban

► **To cite this version:**

Remus Pusca, Raphael Romary, Adrian Ceban. Use of external magnetic field for supervision and diagnosis of electrical traction motors. Nicu Bizon, Lucian Dascalescu and Naser Mahdavi Tabatabaei. Autonomous Vehicles: Intelligent Transport Systems and Smart Technologies, NOVA Publishers, 2014, 978-1- 63321-326-5. hal-04330359

HAL Id: hal-04330359

<https://univ-artois.hal.science/hal-04330359>

Submitted on 8 Dec 2023

HAL is a multi-disciplinary open access archive for the deposit and dissemination of scientific research documents, whether they are published or not. The documents may come from teaching and research institutions in France or abroad, or from public or private research centers.

L'archive ouverte pluridisciplinaire **HAL**, est destinée au dépôt et à la diffusion de documents scientifiques de niveau recherche, publiés ou non, émanant des établissements d'enseignement et de recherche français ou étrangers, des laboratoires publics ou privés.

Use of the External Magnetic Field for Supervision and Diagnosis of Electrical Traction Motors

R. PUSCA^{1,2} R. ROMARY^{1,2} and A. CEBAN^{1,2}

¹Univ Lille Nord de France, F-59000 Lille, France

²U. Artois, LSEE, F-62400 Béthune, France

remus.pusca@univ-artois.fr

raphael.romary@univ-artois.fr

andrian_ceban@ens.univ-artois.fr

Abstract : The work presents a supervision method for detection of AC electrical machine faults, generally used in electrical traction, exploiting the information given by the external magnetic field in the vicinity of the machine. This field is an image of the air-gap flux density and consequently, it contains information concerning the failure presence. In this work, two methods based on the analysis of the magnetic field outside the machine are presented. They are reliable, original, inexpensive and simple to implement in electrical automotive vehicle. They have the advantage of being non-invasive and just get rid from the main drawback presented by other diagnostic methods based on a comparison with a healthy state assumed to be known. The both methods need simple coil sensors placed in particular positions of the motors for flux density measurements. These sensors are simple, non-invasive, low cost and they induce an electromotive force which derivative effect amplifies the low and medium frequencies. These methods are developed in the case of AC electrical rotating machines (induction and synchronous machines) often used in electrical traction. The analysis is focused on the low frequency components of the magnetic field which is not influenced by the presence of electronic converters always used in tractions applications. The theoretical analysis and his experimental validation are also presented.

Keywords: AC motors, electrical traction application, fault diagnosis, low frequency, magnetic field spectral analysis.

1. Introduction

The work presented in this chapter is part of the current concerns in development of the electric traction whose EV (electric vehicle) and HEV (hybrid electric vehicle) are part. Although electric traction is not a new idea, its application to electrical automotive vehicle has be previously abandoned, consequence of an insufficient level of technological development and, recovery today to responds to current problems like the development of a non-polluting vehicle with sufficient reliability and autonomy. In this context, in order to have a chance to succeed, the automotive vehicle should not be a modification of the conventional one. It must be a "new vehicle".

Taking in consideration this remark, the work presented in this chapter show a non-invasive method for supervision and diagnosis of electrical motors used in automotive vehicle. The presence of new traction control systems in the automotive vehicle allows faster control of drive torque and improved dynamic performance [1]. However, these systems require new methods of monitoring and diagnosis to detect the faults because strong vibrations presented in embedded systems reduce the reliability of all system components including electrical machines (motors and generators). To improve the reliability of the "new vehicle" the proposed method, presented in this chapter, can assure a preventive diagnostic based by analyze of the magnetic flux leakage measured outside of electrical machine by non-invasive sensors.

Considering the electrical motor as part integrant of EV and HEV, this chapter presents the used sensors, their positioning around of motor and analysis of measured signals allowing an easy use of the method for supervision and diagnosis of AC (alternating current) motors often used in automotive vehicle. Generally, the electrical motor diagnosis methods require a good knowledge of the machine

and its behaviour in the presence of internal faults. For diagnosis of electrical machines used in classical applications different methods are distinguished [2]:

- diagnostic techniques that rely on knowledge methods and which use usually the artificial intelligence. These methods are enriched by feedback and not require the mathematical model of a failure machine.

- methods of identification and estimation of the physical parameters of the machine. In this case, monitoring is established by comparing the measurement results with those obtained by analytical modelling or by calculation of a state vector.

- methods based on signal modelling. These methods analyze the time evolution or the spectral content of the different measured signals in order to detect a fault of the electrical machine.

Today many works are dedicated to motor fault analysis using different methods as the current signature analysis [3,4,5], exploitation of the slot harmonics [6,7], artificial intelligence techniques [8], vibrations and noise measurement [9,10,11] or flux analysis [12,13,14] and all of these techniques have been validated beyond the research laboratories in order to find their place in industry [15]. It could be interesting to know if these methods can be implemented in electric traction motors in order to diagnose incipient faults because, in electric traction, the speed variation is often assured by static converters which feed the motors with adapted waveforms of the currents. These signals are generally not perfectly sinusoidal and are source for electromagnetic disturbances. Moreover, the interpretation of the results obtained from these methods requires a level of expertise advanced which makes it difficult a real democratization of these techniques among users of electrical machines. Indeed, only systems where a breakdown of the machine can have disastrous consequences (e.g. the electricity generating plant) are equipped with a supervision system.

Generally, all diagnostic methods require knowledge of the healthy state of the machine regardless of the physical exploited parameter. The fault detection is then based on the comparison of a given state signature with that of the healthy state assumed to be known, considering an indicator sensitive to a particular defect. The difficulty with this approach is that, often, the sensitive indicators already exist for the healthy machine (case of a spectrum lines). It is then their change, often the increase, which is likely to provide information on the presence of a fault. On the other hand, the load of the machine can be considered for diagnostic as a disturbing factor, because it induces several healthy states. Additional difficulty lies in the fact that the supposed healthy state is almost never known before that the failure appears, because the operator of the machine has not taken the precaution to record the parameters that characterize the healthy machine.

Recently, methods based on the analysis of the external magnetic field have appeared, they have the advantage of being non-invasive and easy to implement [16,17,18]. These techniques exploit information in the stray field around the machine in order to respond to industrial problems concerning the diagnosis [19], but also on monitoring the aging of insulation or the monitoring of eco efficiency [20, 21]. The different applications differ in the frequency range to be analyzed.

The current diagnosis techniques exploiting the range of low and medium frequencies, up to the slotting effect of the electric machine, give the possibility to detect the stator faults (inter-turn short circuit) and rotor faults (broken bars, inter-turn short circuit) by analysis of the external magnetic field of induction and synchronous machines. At the base of these techniques, there is an analytical model, which shows the decomposition of the external magnetic field into a radial and axial field does not have the same properties, because each has a different origin. This model predicts the spectral components of the stray field affected by different faults.

The work presented in this chapter is part of this category, mainly considering the effects of a fault on the magnetic stray field and it is adapted toward the diagnosis of rotating electrical machines including electric traction motors since it is not influenced by the static converters and use the load working for the detection of the faults. Nowadays, rotating electrical machines are presented in all areas of modern life including the electrical vehicle and one of the most important objectives of the maintenance systems is the detection of incipient faults in order to anticipate a shutdown of the system. In this work, two methods based on the analysis of the magnetic field outside the machine are presented. They are reliable, inexpensive, simple to implement and non-invasive. These methods are developed in the case of AC electrical rotating machines (induction and synchronous machines). The analysis focuses on the magnetic field dispersion in the vicinity of the machine, especially its radial and axial distribution which presents different sensitivity according to various faults.

For application of these methods in electrical traction, two coil sensors are used to measure the stray field in the motor vicinity (Fig. 1). These sensors induce an **electromotive force (emf)** which derivative effect amplifies the low and medium frequencies. They are simple to carry out, non-invasive and low cost. Moreover, they can be set up outside the motor without needing large place in electrical system of hybrid vehicles. The diagnosis procedure is able to indicate the failure presence and can be implemented within a simple microcontroller. For diagnosis, each fault gives specific signature that are identified and analysed.

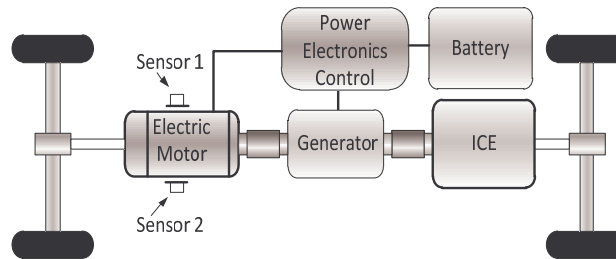


Fig. 1. Positions of sensors for on-line supervision of HEV traction motor.

Two diagnosis methods are developed in this work. The first method concern the inter-turn short-circuit faults in the stator winding. It uses two external flux coil sensors placed in particular positions that measure the external magnetic field, the signal delivered by the both sensors being exploited for diagnosis. The analysis concerns the magnitude of specific harmonics of the electromotive force delivered by the coil. One will be interested in the magnitude of the third rank harmonic for Salient Synchronous Machines and the rotor slotting harmonics for Induction Machines. This method does not require any knowledge of a presumed machine's healthy former state, it's originality is the use of the load to improve the diagnostic. Here, the load is not longer a disturbing factor but it is used for the fault discrimination. Actually a comparison between machine operating conditions (no-load and load) enables to detect a stator fault.

The second method is based on the variations of the axial flux density in the presence of rotor faults. Any changes of magnetic circuit conditions, such as a broken bar or the formation of an eccentric air-gap due to bearing wear, will, by the same token, be reflected with a corresponding change in the axial flux. The analysis is focused on the low frequency components of the magnetic field, which are not influenced by the presence of electronic converters usually used in industrial and traction applications and which are less attenuated during their penetration through the stator magnetic core or the machine external frame. The both methods need simple coil sensors for flux density measurement.

In the end of the chapter experimental implementation of the sensors and results are presented. The faults have been artificially created in the rotor and stator on different AC machines, special designed for the tests in order to present the experimental results of the suggested diagnosis methods.

2. Magnetic field

From a diagnostic point of view, the advantage of methods based on measurement of the external magnetic field is that they are non-invasive. These methods are simple to implement and they use a sensor placed near the electrical machine, able to measure the external magnetic field. Considering the position of the sensor, the measured of dispersion field does not originate from the same source, and not result, necessarily from the same physical phenomenon [22].

2.1 Measurement of external magnetic field

In a rotating electrical machine, the leakage flux is created by the different elements of the machine. A distribution of these field lines is shown in Fig. 2 [23].

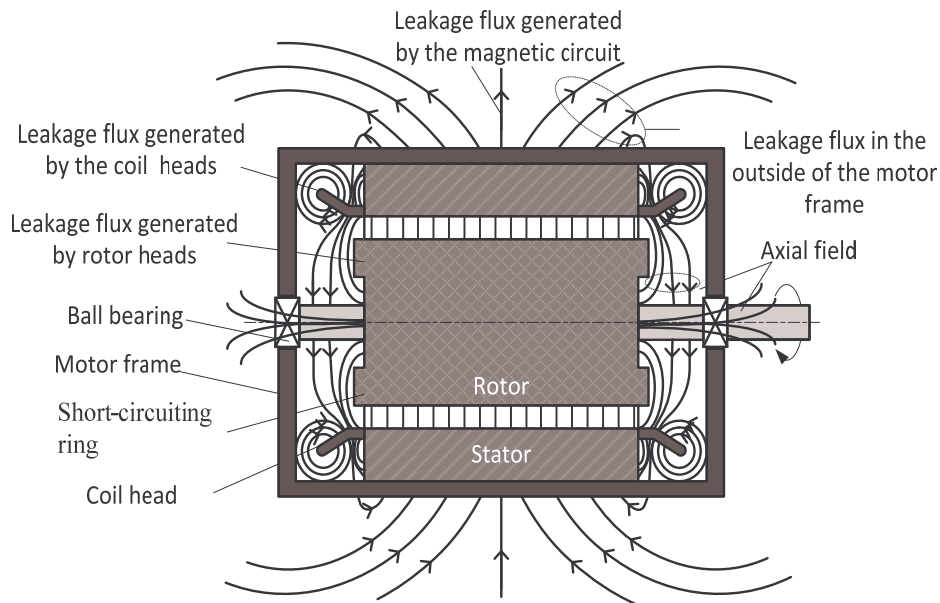


Fig. 2. Distribution of leakage flux lines in electrical machine

From this distribution, we can decompose the external field in two parts called axial and radial field. These two fields are combined to form the leakage field: the axial field in a plane that includes the axis of the machine and the radial field in a plane perpendicular to the axis of the machine. The leakage field may give information about the presence of a fault, and sometimes its location. Figure 3 shows the different positions for measurement of the leakage field using a coil sensor. Assuming the field lines shown in Fig. 3, the sensor will be sensitive to different components of the field and the measured signal will depend on the position of the coil:

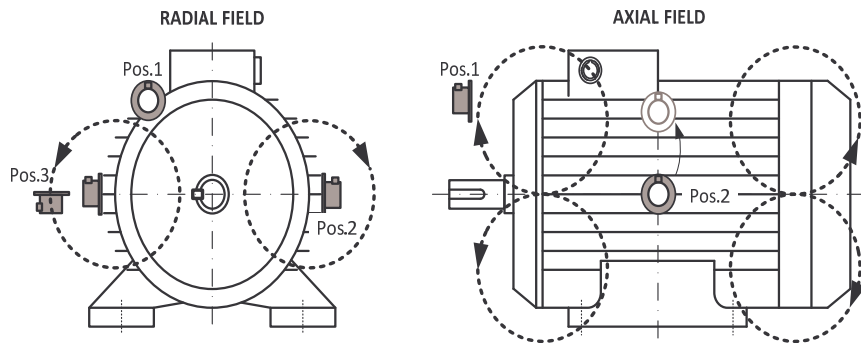


Fig. 3. Measure of leakage field in near vicinity of the machine

-in position 1 (Pos. 1), the coil measures the axial field. In this case the amplitude of the measured flux is maximum at the motor endshield (around heads of the windings), and minimum at the middle of the machine length; this minimum is practically null.

- in position 2 (Pos. 2), the coil measures the normal component of the radial field. Taking the coil sensor away from the motor endshields increases the sensitivity to the air gap flux density.

-in position 3 (Pos. 3), the coil is used to measure the external field called "pure radial" sensitive to the tangential component. In theory, field lines generated by the winding heads cannot cross the section of the coil sensor in this position.

2.2 Measurement sensors

Several types of sensors can be used to measure the external field (magneto-resistive sensor, Hall effect sensor, coil sensor ...).

In the diagnostic method presented in this chapter, the coil sensor is used. The principle of the coil sensor is to measure the field embraced by a coil located in the vicinity of the electrical machine [24]. The sensor provides an emf equal to the derivative of the magnetic field with respect to the time; however, the measurement is only possible for the variable fields. With this type of sensor, the measurement is simple and direct because it does not require associated electronics, unless it is necessary to amplify the induced emf signal [22]. The performance of the measurement depends on the size of the sensor. The main advantage of these sensors is their simple design which allows users to make it according to their needs [25]. The sensor used for experimental tests and its frequency response are represented in Fig. 4.

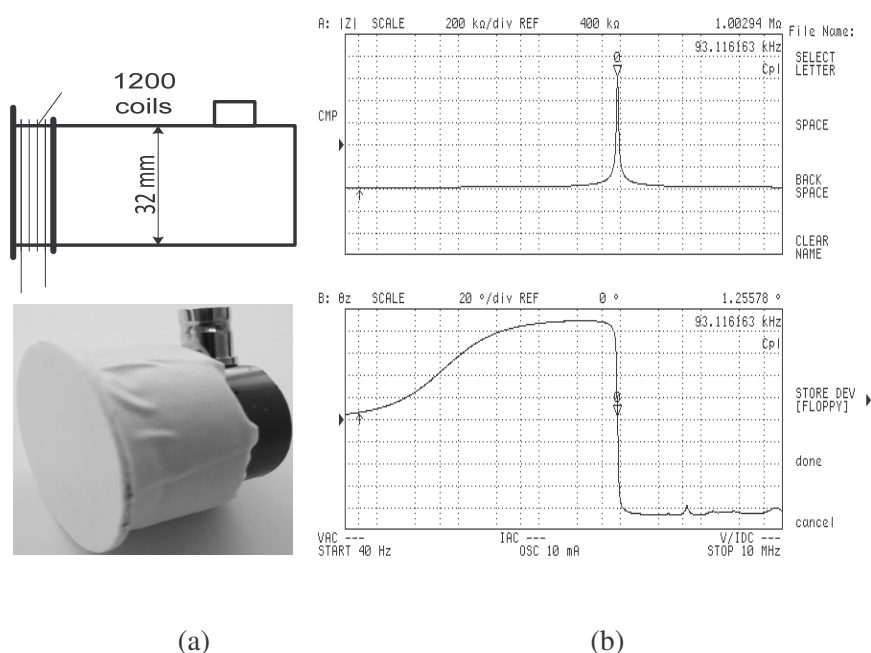


Fig. 4. Coil sensor: (a) photo; (b) frequency answer

This small sensor will be used for all experimental measurements presented in this work. It was built for small and low power machines. The coil diameter is about 3.2 cm and it has 1200 turns. Its frequency response shows a resonance at 93 kHz, so, the sensor is suitable to be used for measurement of the field in a frequency range lower than this frequency, what actually corresponds to the frequency range exploited by proposed diagnosis methods. This type of sensor is used for flux measurements because it is simple, non-invasive, low cost, induces an emf with a natural derivative effect that amplifies the low and medium frequencies [26].

3. Stator faults in AC electrical rotating machines

The most of stator faults are attributed to the degradation of insulation. They manifest themselves as a short-circuit between turns, by a short circuit between two phases or by a short-circuit between a phase and the ground. In this paragraph the analytical model presented is developed for the short-circuit between the turns of the same phase because it is a common defect that can occur either at the coil ends or in the notches, causing a decrease of effective winding turns. On the other hand, it leads to increase the stator current in the affected phase and to a slight variation of the amplitude in the others. In the case of induction machines, it amplifies also the current in the rotor circuit [27, 28]. Thermal

stress caused by short-circuit can cause the spread of the fault to other coils and the complete destruction of the machine.

The developed analytical approach makes it possible to identify the properties of the airgap flux density waves generated by the fault and proposes a diagnostic method based on those.

3.1 Analytical model

For analytical study of stator faults in AC motors, a simplified geometry of the machine has been considered (Fig. 5) to study the external magnetic field.

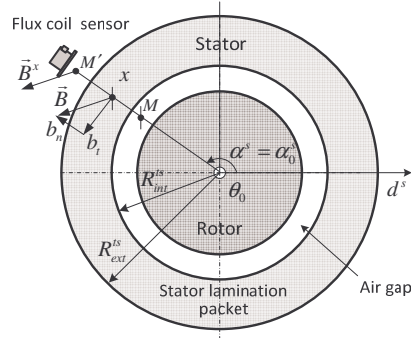


Fig. 5. Transverse section and considered parameters of simplified machine

The point M' outside the machine has polar coordinates x, α^s . The stator is composed of a magnetic yoke and an external frame; the gap which can possibly exist between the stator yoke and the external frame is neglected. To simplify, the considered machine presents smooth airgap where the flux density is imposed. Fig. 5 also gives the position of the sensor, placed at the level of the point M . Here the R_{int}^{ls} and R_{ext}^{ls} are internal and external radii of the stator.

For short-circuit model let us consider $p = 2$ pole pair, three-phase stator winding machine given in Fig.6 [26]. Each coil is made up of m^s elementary coils of n^s / m^s turns, where n^s is the machine per phase, per pole pair turn number. As the coil of the same phase are series connected it results that the per phase turn number is pn^s .

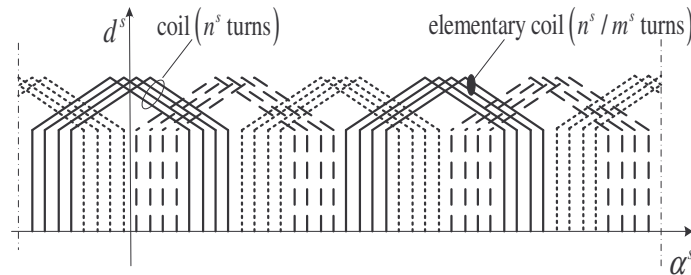


Fig. 6. Three phase stator windings ($p = 2$)

Let us suppose that y turns among n^s / m^s of an elementary coil of the phase q are short-circuited. If y is small compared to pn^s , it is possible to consider that the i_q^s currents are unchanged. This assumption makes it possible to characterize inter-turn short circuit by implementing a model which preserves the initial structure of the machine. This model considers that the faulty stator winding is equivalent to the healthy winding, plus y short-circuited turn coil which is denoted “additional coil”. A i_{qf}^s fictitious current circulates in this coil, which is composed of inter-turn short circuit induced current i_{sc}^s and the current in opposite direction i_q^s :

$$i_{qf}^s = i_{sc}^s - i_q^s \quad (1)$$

A damaged elementary coil is shown in Fig. 7. This approach makes it possible to separate the effects of the fault while preserving the initial structure, what simplifies the fault analysis. In this way, the resulting air-gap flux density b^* can be expressed as:

$$b^* = b + b_{qsc}^s \quad (2)$$

with $b = \sum_{K,H} b_{K,H}$,

where $b_{K,H} = \hat{b}_{K,H} \cos(K\omega t - H\alpha^s - \varphi_{K,H})$ (K is the frequency rank and H the polarity of $b_{K,H}$) and b_{qsc}^s is generated by the damaged coil.

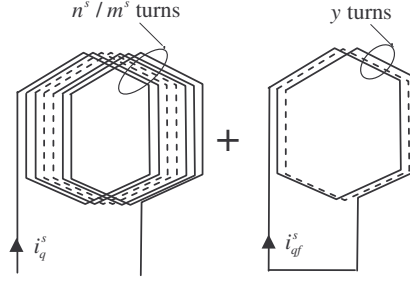


Fig. 7. Elementary coil with y short-circuited turns

To determine b_{qsc}^s , the \mathcal{E}_{qsc}^s mmf generated by the additional coil must be defined. The \mathcal{E}_{qel}^s mmf generated by two healthy elementary coils of the same phase, connected in series and shifted of π , is presented in Fig. 8 (a). The Fig. 8 (b) gives the mmf generated by the faulty turns.

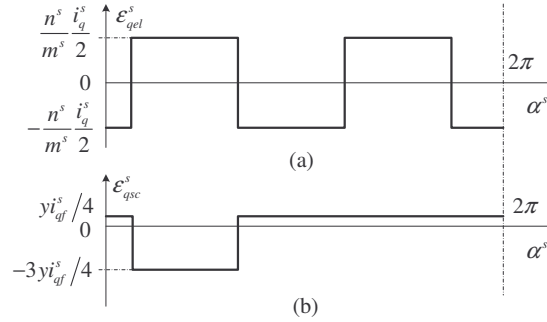


Fig. 8. Mmf components generated by elementary damaged coil created by: (a) two healthy elementary sections; (b) y short-circuited turns

The particularity of this result concerns the \mathcal{E}_{qsc}^s mmf generated by the additional coil which is a unidirectional wave, although \mathcal{E}^s is a rotational one. Also, its polarity H is equal to 1 that produces a dissymmetry in the stator mmf wave.

In the stator reference frame d^s which is confounded with the stator phase 1 axis, \mathcal{E}_{qsc}^s can be written as the sum of rotational mmf waves evolving per pair in opposite directions:

$$\mathcal{E}_{qsc}^s = I_f^s \sum_h A_h^s \cos(\omega t - h\alpha^s - \varphi_h) \quad (3)$$

where I_f^s is the rms value of i_{qf}^s , ω is the angular frequency, h is a not null relative integer, which takes among others, all the values of h^s which is defined by: $h^s = 6k + 1$ (k is an integer which varies between $-\infty$ to $+\infty$). A_h^s is a function that takes into account the winding coefficient tied to

the rank h^s . φ_h is the phase which depends on the position of the elementary coil concerned by the short-circuit but also of the phase where the short-circuit occurs.

The flux density b_{qsc}^s generated by the fault is obtained by multiplying ε_{qsc}^s with air-gap permeance λ expressed by:

$$\lambda = \sum_{k^s=-\infty}^{+\infty} \sum_{k^r=-\infty}^{+\infty} \Lambda_{k^s k^r} \cos \left[(k^s N^s + k^r N^r) p \alpha^s - p k^r N^r \theta \right] \quad (4)$$

where $\Lambda_{k^s k^r}$ is a coefficient which depends on the ranks k^s and k^r and the air-gap geometry, N^s is the stator per pole pair tooth numbers.

3.2 Model for salient-pole synchronous machine

For a healthy salient-pole synchronous machine, K and H are defined as:

$$\left. \begin{aligned} K &= 1 + 2k^r \\ H &= p(h^{sr} + k^s N^s + 2k^r) \end{aligned} \right\} \quad (5)$$

where h^{sr} includes all the values taken by h^s and h^r : $h^{sr} = h^s \cup h^r$ and $h^s = 6k + 1$; $h^r \in (1, 3, 5, \dots, +\infty)$.

If a fault exists, the flux density b_{qsc}^s can be expressed as:

$$b_{qsc}^s = \sum_{K_{sc}, H_{sc}} \hat{b}_{sc, K_{sc}, H_{sc}} \cos \left(K_{sc} \omega t - H_{sc} \alpha^s - \varphi_{sc, K_{sc}, H_{sc}} \right) \quad (6)$$

with:

$$\left. \begin{aligned} K_{sc} &= 1 + 2k'^r \\ H_{sc} &= h + p k'^s N^s + 2p k'^r \end{aligned} \right\} \quad (7)$$

k'^s and k'^r are equivalent to k^s and k^r . Consequently they vary from $-\infty$ to $+\infty$.

The resulting flux density appears, after attenuation, at the level of the external transverse field. That results in the presence of harmonics at $K\omega$ and $K_{sc}\omega$ angular frequencies in the signal delivered by the flux sensor. Considering K and K_{sc} the values calculated by (5) and (7), it is possible to make the following remarks:

- K_{sc} does not bring new frequencies and the failure presence will be appreciated through the variation of the amplitudes of existing lines in the healthy machine spectrum.
- the sensitive spectral lines are in low frequencies. Indeed, the corresponding harmonics for $k'^r = \pm 1$, are ω and 3ω . Consequently, one of these components is confused with the fundamental [12].
- Other sensitive spectral lines ($k'^r = \pm 2, k'^r = \pm 3, \dots$) are superimposed on the components at angular frequencies $3\omega, 5\omega, 7\omega, \dots$; that may exist for a healthy machine (supply harmonic, saturation).

These properties make difficult the diagnosis by analysis of the changes in the amplitudes of the measured components. In the following the properties relating to the dissymmetry generated by the fault will be exploited.

3.3 Model for induction machine

Under healthy conditions the quantities K and H in the case of induction machine can be expressed by:

$$\left. \begin{aligned} K &= 1 + k^r N^r (1 - s) \\ H &= p(h^s + k^s N^s + k^r N^r) \end{aligned} \right\} \quad (8)$$

The sensitive lines to the fault are characterized by the quantities K_{sc} and H_{sc} defined as follows:

$$\left. \begin{aligned} K_{sc} &= 1 + k'^r N^r (1 - s) \\ H_{sc} &= h + p(k'^s N^s + k'^r N^r) \end{aligned} \right\} \quad (9)$$

A numerical application for induction machine is presented in annexe. The results obtained by compilation show that each harmonic of the external field, at given k^r is essentially created by components with the lowest possible polarities. The analysis will focus on the diagnosis harmonic at 850 Hz, because it is generated by a component with the lowest polarity both for the healthy machine and for the faulty machine ($H = -2$, $H_{cc} = -1$). As shows the numerical application (annexe 1) this harmonic has a high amplitude value and can be more easily measured at the outside of motor frame.

3.4 Principle of the tests

For the new diagnosis method, which exploits the change of external magnetic field in presence of the faults, the measurements are carried out in two diametrically opposed positions: $\alpha_1^s = \beta_0$ (Pos.1) and $\alpha_2^s = \beta_0 + \pi$ (Pos.2), (Fig. 9).

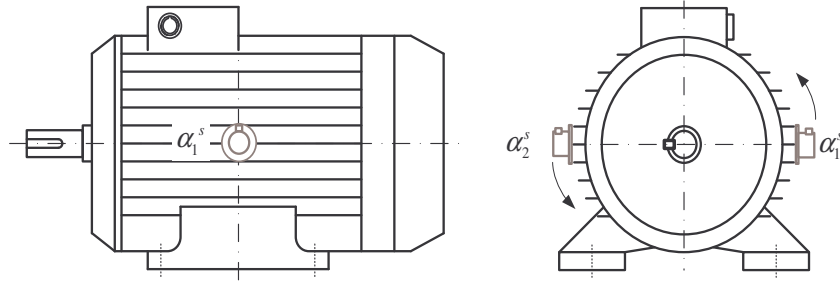


Fig. 9. Sensors position for measurement of external magnetic field

The principle of the method consists in the analysis of the variations induced by the fault at the level of particular harmonic components measured in the both positions. The corresponding flux density components must have significant amplitude in the external magnetic field. Consequently, taking into account the magnitude of the air-gap flux density and considering the attenuation of these components in the stator core, one will be interested in the components defined by the lowest values of h^s , h^r , k^s , k^r , k'^s , k'^r leading to the smallest as possible value of H .

The respect of these constraints leads to consider the spectral line at ω angular frequency ($K=1$) of magnitude $\hat{b}_{1,1}$. However, this component corresponds to the fundamental of the air-gap flux density which generates the main effects: $\hat{b}_{1,1} \gg \hat{b}_{1,H}$ with H different from 1. It results that \hat{b}_1 will be not very sensitive to the components defined for $|H| > 1$.

In the case of *salient-pole synchronous machine*, the analysis will be focused on the spectral lines related to $K = 3$, (line at 150Hz). For a four pole machine ($p = 2$), the flux density components that contribute to this harmonic are defined as follows:

- for healthy machine: $h^r = 1, k^s = 0, k^r = 1, h^{sr} = 1$ in (5), which gives $K = 3$ and $H = 3p = 6$;
- for faulty machine: $h = -3, k^s = 0, k^{r'} = 1$ in (7), that leads to $K = K_{sc} = 3, H_{sc} = -1$.

The flux density component b_3^{*x} at 3ω angular frequency on the outside of the machine is the sum of a term relative to the healthy machine (of amplitude \hat{b}_3^x) and a term relative to the faulty machine (of amplitude \hat{b}_{cc3}^x). In Pos.1, the resulting component can be expressed as:

$$b_3^{*x(1)} = \hat{b}_3^x \cos(3\omega t - 6\beta_0 + \varphi_3^x) + \hat{b}_{cc3}^x \cos(3\omega t + \beta_0 + \varphi_{sc3}^x) \quad (10)$$

In Pos.2, it becomes:

$$b_3^{*x(2)} = \hat{b}_3^x \cos(3\omega t - 6\beta_0 + \varphi_3^x) - \hat{b}_{cc3}^x \cos(3\omega t + \beta_0 + \varphi_{sc3}^x) \quad (11)$$

The difference between the both positions is tied to the sign which precedes the component due to the fault. For a healthy machine such as $\hat{b}_{sc3}^x = 0$, the components defined by (10) and (11) present the same amplitude. Under fault conditions, the amplitude of the component in one of the positions increases whereas the other one decreases. Practically, it can observe differences between measurements for the both positions, even in the healthy case: $\hat{b}_3^{x(1)}$ in Pos.1 is different from $\hat{b}_3^{x(2)}$ in Pos.2. Two external causes can be responsible for this dissymmetry:

- Pos.1 and Pos.2 cannot be perfectly symmetrical from each other.
- the machine realization techniques can lead to a dissymmetry causing different attenuation coefficients at the level of the two sensor positions.

In this case, the method can be extended thanks to the exploitation of a test in load. The method can be refined as following:

Under healthy conditions, at load, the stator current increases but, at given supply voltage, the air-gap flux density stays practically identical to that obtained at no-load. As the external elements responsible of the attenuation act in the same way in Pos.1 and Pos.2 for the no-load and for the load tests, the amplitudes $\hat{b}_3^{x(1)}$ and $\hat{b}_3^{x(2)}$ keep similar values or at least evolve in the same way when the machine is loaded.

Under faulty conditions, at load, \hat{b}_{sc3}^x varies taking into account the model chosen to characterize short-circuit (the loading current contributes to the definition of the fictitious current which circulates in the damaged coil). Consequently, according to (10) and (11), the magnitude of the component at 3ω angular frequency in Pos.1 and Pos.2 will evolve in opposed directions. The variations of the lines at 3ω are thus an indicator of defect. The advantage of the method is that it does not require any knowledge of a healthy state to detect the fault.

In the case of *induction machine*, the lines are located in a frequency range where they can be easily identified. The analysis is focused on the line at 850Hz because it is relative to a flux density component having a low pole pair number as well for the healthy case as for the faulty one.

- for healthy machine: $k^r = 1, k^s = -1, h^s = 7$ lead to $K = 17, H = -2$ in (8)
- for faulty machine: $k^{r'} = 1, k^s = -1, h^s = 15$ lead to $K_{sc} = 17, H_{sc} = -1$ in (9).

Relations similar to (10) and (11) are obtained, but by taking $K = K_{sc} = 17$ (instead of 3) and $H = -2$ (instead of 6).

4. Rotor faults in AC electrical rotating machines

This section briefly presents the main phenomena characterizing the rotor faults. It will focus on the influence of a broken bar on the change of the external magnetic field of an induction machine.

An analytical approach requires some simplifying assumptions but will allow one to give the specific harmonics of the fault, including their frequency and polarity. The analytical study will highlight the need to consider the axial field as part of leakage flow for which a simplified model will be proposed and a specific signature for this fault type, visible in the spectrum of the external magnetic field.

4.1 Types of the rotor faults

4.1.1 Bearings faults

The majority of faults in electrical machines are relative to bearing defects that have mechanical causes (lubrication, fatigue, etc.) or electrical (circulation of leakage currents induced by the converters [29]) and leads to more general mechanical effects such as increased noise and vibration by the appearance of the movements of the rotor about the longitudinal axis of the machine [30]. This type of faults induces also variations (oscillations) of the load torque. The ultimate point of the bearing defect is the rotor blocking.

4.1.2 Eccentricity

The eccentricity of an electric machine is a phenomenon that evolves over time and exists from its manufacture. It passes through various stages of fabrication and assembly tolerances, which induces to decentre the rotor relative to the stator. During operation of the machine, two main causes increase rotor eccentricity. The first is inherent to the system shaft in which the machine operates and can impose a radial force on the shaft of the machine. This can lead to bearing wear and amplification of the eccentricity. The second phenomenon that may exacerbate the eccentricity is itself inherent to the operation of the machine. Actually, the shift creates an unbalance in the distribution of radial forces between the stator and the rotor [31, 32]. The ultimate point of eccentricity is the friction between stator and rotor, which is synonymous of fast destruction of the machine.

4.1.3 Broken bar

Inter-turn short circuit fault may also occur in a wound rotor. For squirrel cage induction machines, broken rotor bars and the breaking of the short-circuit rings are the most common rotor failures (Fig. 10).

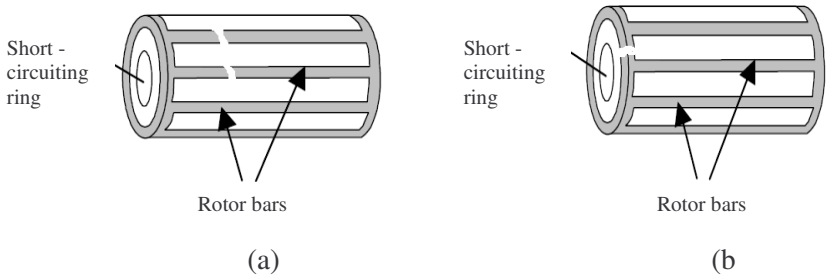


Fig. 10. Fault of squirrel rotor cage: (a) broken bar ; (b) breaking of the short-circuiting ring

The broken bar or the breaking of the short-circuit rings may be due, for example, to mechanical overload (frequent starts, etc.), to excessive local heating or to a manufacturing defect (air bubble or bad welds). This generates oscillations of currents and electromagnetic torque even more apparent when the inertia of the system has a high value (constant velocity) [33,34]. If the system inertia is lower, oscillations appear on the angular speed and the amplitude of the stator currents. The occurrence of a broken bar does not cause an immediate breakage of the machine, because the current crossing the broken bar spreads over the adjacent bars. Therefore, these bars are overloaded and the thermal and electromechanical constraints can lead to their breaking and so on until the breakage of a sufficiently large number of bars to stop the machine.

4.2 Rotor broken bar

4.2.1 Influence on the speed variation

The presentation of the phenomenon will consider only the flux density component of p pole pairs. Under healthy operating conditions, the balanced three-phase current system creates a fundamental clockwise rotating magnetic field in the air-gap. This field induces a current in the rotor bars with a frequency proportional to the rotor slip s . The rotor bars then generate a clockwise field rotating at $s\Omega_s$ in a rotor referential (Fig. 11 (a)). For a symmetrical motor (healthy machine), there is not any anticlockwise field in the air-gap [35, 36].

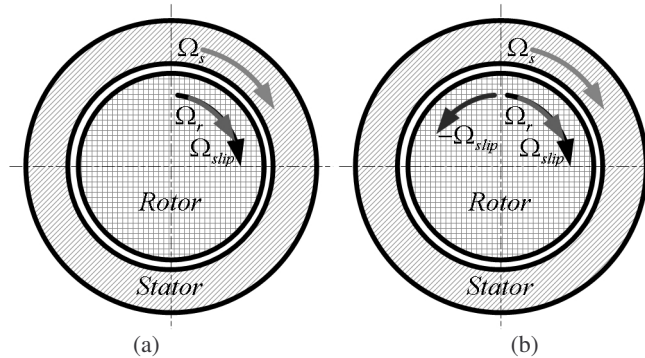


Fig. 11. Operation schema for: (a) healthy motor; (b) faulty motor

Under rotor faults, in addition to the clockwise field an anticlockwise field appears, created by the unbalance of rotor bar currents and which rotates at an angular velocity $-s\Omega_s$ shown in Fig. 11 (b). It is possible to associate with this anticlockwise field a negative-sequence current system with amplitude I_m , which is added to the positive-sequence current system with amplitude I_p .

Figure 11 (b) shows the phenomenon due to the appearance of rotor failure. A flux density component rotating at Ω_{fault} appears in the stator referential:

$$\Omega_{fault} = \Omega_r - s\Omega_s = \Omega_s (1 - 2s) \quad (12)$$

which leads to the well-known frequency in literature f_{fault} , appearing in the radial external magnetic field and in the line current:

$$f_{fault} = (1 - 2s)f \quad (13)$$

The interaction of the rotor currents with the clockwise stator field produces the electromagnetic torque. In case of broken rotor bar fault, the total torque can be expressed as follows:

$$C_{e_tot} = C_{e_srp} + C_{e_srn} = \pi \frac{RLe_m}{\mu_0} k_s I_s \left[k_r I_{rp} \sin(\varphi_{B_s} + \varphi_{B_{rp}}) + k_r I_{rn} \sin(2s\omega t + \varphi_{B_s} - \varphi_{B_{rn}}) \right] \quad (14)$$

where C_{e_srp} represents the mean torque due to the interaction of the stator and the rotor fields in the clockwise direction, C_{e_srn} is the pulsating torque of pulsation $2s\omega$ due to the interaction of the stator clockwise field with the anticlockwise rotor field; φ_{B_s} , $\varphi_{B_{rp}}$ and $\varphi_{B_{rn}}$ are respectively the phases relative to the stator phase one current of the stator flux density, the rotor flux densities in the clockwise direction and in the anticlockwise direction; k_s is a coefficient that depends on the stator winding arrangement and k_r is a coefficient that depends on the rotor cage constitution.

The torque oscillation at frequency $2sf$, also presented in [35], generates a speed oscillation at this frequency whose amplitude depends on the rotor asymmetry, the motor load level [36,37], and the total moment of inertia J . The speed is calculated with the relation:

$$J \frac{d\Omega_r}{dt} = C_{e_tot} - C_r = C_{e_srn} \quad (15)$$

where C_r is the load torque:

$$\Omega_r = \frac{1}{J} \int C_{e_srn} dt + \Omega_0 \quad (16)$$

By calculating the integral (11) one obtains:

$$\Omega_r = \Omega_0 + \Delta\Omega_r \cdot \cos(2s\omega t + \varphi) \quad (17)$$

where $\Delta\Omega_r = -\pi k_s I k_m I_m \frac{1}{2sJ} \cdot \frac{RLe_m}{\mu_0}$ is the magnitude of the speed oscillation, Ω_0 is the mean value of Ω_r which changes in the dependence on the number of broken bars at given load torque, and $\varphi = \varphi_{B_s} - \varphi_{B_{rn}}$.

It is well known that the speed oscillation also generates an additional air-gap flux density component at $(1+2s)f$.

4.2.2 Influence on the axial flux

For the modeling of the axial field, it is necessary to consider the field lines existing at the machine extremities. The distribution of these ones strongly depends on the geometry and the mechanical components that exist at the machine extremities. As mentioned in [33], the total axial flux Φ_{AT} outside the induction machine with an eccentricity fault can be written in the following form:

$$\Phi_{AT} = \hat{\Phi} \cos(\omega t - p\beta) \quad (18)$$

with $\beta = \beta_0 + \Omega_r t$, β indicates the position of the minimum air-gap thickness. Under broken rotor bar fault, a speed variation appears and will influence the external axial flux. In this case (18) can be written as follows:

$$\Phi_{AT} = \hat{\Phi} \cos[\omega t - p(\beta_0 + \Omega_r t)] \quad (19)$$

Developing the argument of the cosine, using (17) one obtains:

$$\Phi_{AT} = \hat{\Phi} \cos[s\omega t - \Delta\Omega_r p t \cos(2s\omega t + \varphi) - p\beta_0] \quad (20)$$

A frequency modulation appears in Φ_{AT} . The time variation of (20) for $\hat{\Phi} = 1\text{Wb}$, $\Delta\Omega_r = 1\text{ rad/s}$ and $s = 2.5\%$ is presented in Fig. 12 (a). A direct analysis of the signal is difficult; hence the change in the frequency domain is performed by Fast Fourier Transform (FFT). The obtained spectrum is given in Fig. 12 (b).

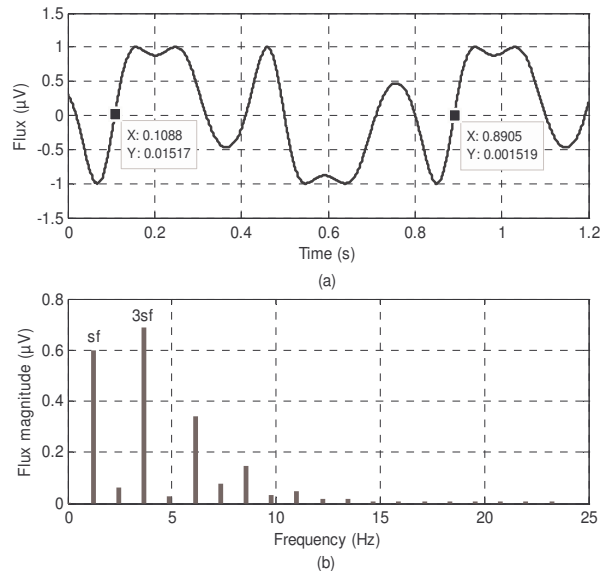


Fig. 12. Simulation of axial flux variation: (a) axial flux signal; (b) FFT for the axial flux

In the spectrum it can be observed the appearance of the harmonic $3sf$ due to the speed variation and sf due to dynamic eccentricity on the axial flux. One can notice that a small speed variation can produce an important component at frequency $3sf$. With the considered speed variation that corresponds approximately to 2 broken bars; the component $3sf$ is higher than the initial component sf .

5. Experimental tests

5.1 Achievements of the tests

The application of proposed methods for stator faults is presented considering the test carried out on a salient-pole synchronous machine and an induction machine. For rotor faults an experimental bench using two identically squirrel-cage induction motors (one healthy and another with a broken bar) is used. The principle of measurement is shown in Fig. 13

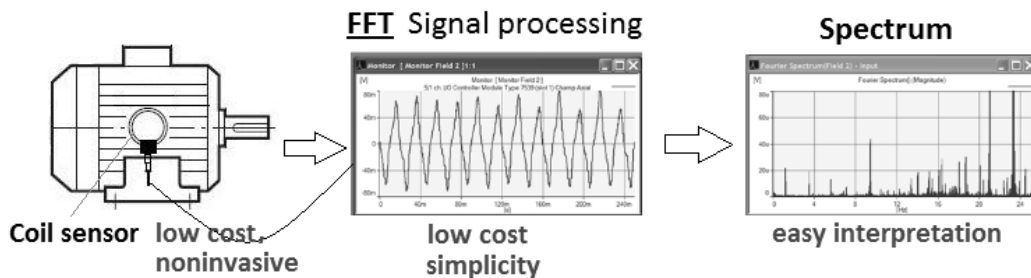


Fig. 13. Measurement and treatment of emf signal

5.2 Stator tests

5.2.1 Inter-turn short circuit in synchronous machines

The application of the proposed method is presented considering a test carried out on a salient-pole synchronous machine characterized by: 7.5 kW, 50 Hz, $p = 2$, 230 / 400V, $N^s = 18$, grid connected. This machine has been rewound so that the terminals of the different stator elementary sections are extracted from the winding and are brought back to a connector block which is fixed above the machine as indicated in Fig. 14. So it is possible to produce short-circuits between elementary coils.

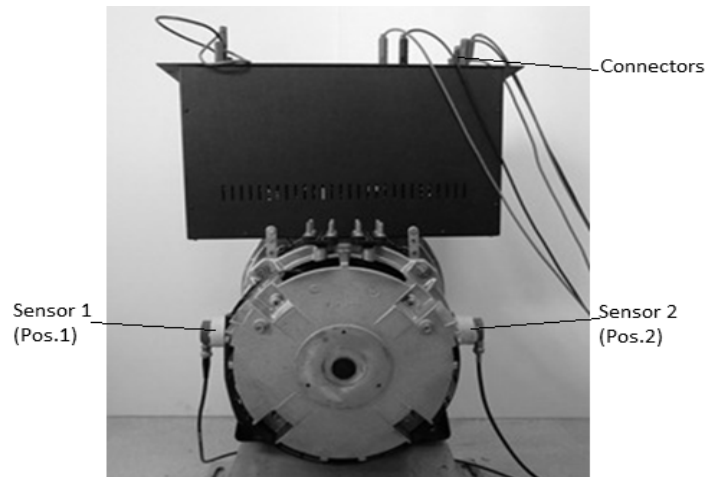


Fig. 14. Modified salient-pole synchronous machine and the sensors' positions

The tests consist in measuring and analyse the emf delivered by the sensors in order to validate the suggested procedure when an elementary coil is short-circuited (what corresponds to 16,6% of the whole winding of a phase). In order to avoid total damage of the winding, the short-circuit current is limited by an external resistance R . Verification have also be done in order to make sure that the currents in the wires going up from the machine towards the connector block do not disturb the measurements. Pos.1 and Pos.2 correspond respectively to β_0 and $\beta_0 + \pi$, β_0 is chosen in the axis of the tested phase. The interest is focused on the harmonic at 150 Hz. Figures 15 a and b shows the variations of the harmonic at 150 Hz relative to the healthy machine (motor) when the state (marked with arrow) varies from no-load to load.

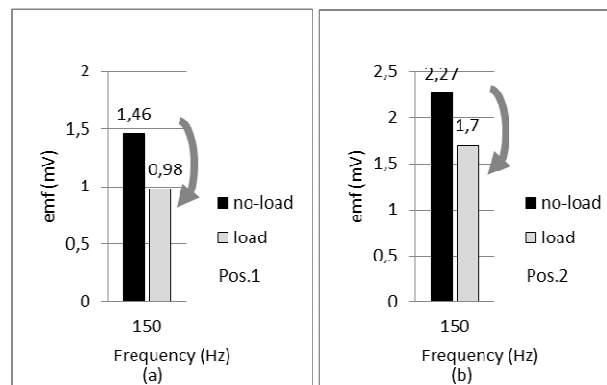


Fig. 15. Harmonic components at 150 Hz for a healthy salient-pole synchronous machine (motor) at no-load and load operations.

It can be observed here that the magnitudes vary in the same way (decrease) for the two positions. Under faulty conditions at full load (Fig. 16) it can be observe that the magnitudes in both positions vary in the opposite ways. This indicates the failure presence and confirms the proposed method.

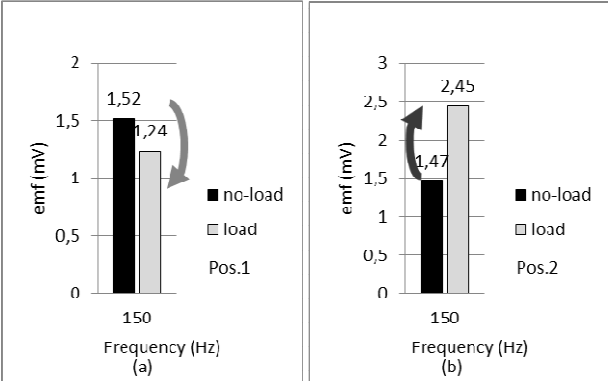


Fig. 16. Harmonic components at 150 Hz for faulty salient-pole synchronous machine (motor) at no-load and load operations.

Another interest is the limit of the method. The tests are realised on the machine which operates as generator. The corresponding results are shown in Fig.17 and Fig.18. One can remark the same phenomenon: under healthy case the magnitudes varies in the same direction, but in the faulty case they vary in opposite direction.

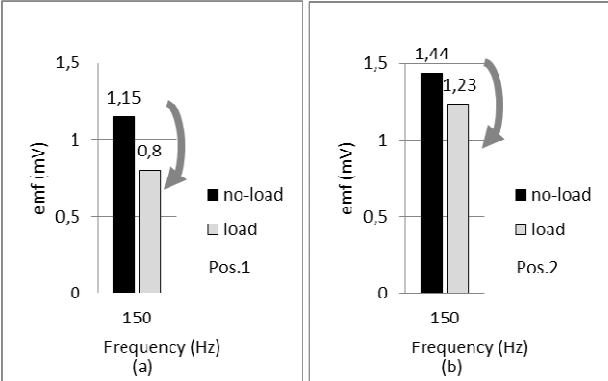


Fig. 17. Harmonic components at 150 Hz for a healthy salient-pole synchronous machine (generator) at no-load and load operations

The next test has been realized on a four pole, 4,4 kW, 50 Hz 3 × 380 V permanent magnet synchronous motor. The obtained results under healthy and faulty conditions are given in Fig. 19 and Fig 20. It can be observed that under healthy case the harmonic magnitudes at 150 Hz vary in the same direction, but when the inter-turn short circuit exists in the stator winding these harmonic magnitudes vary in different direction.

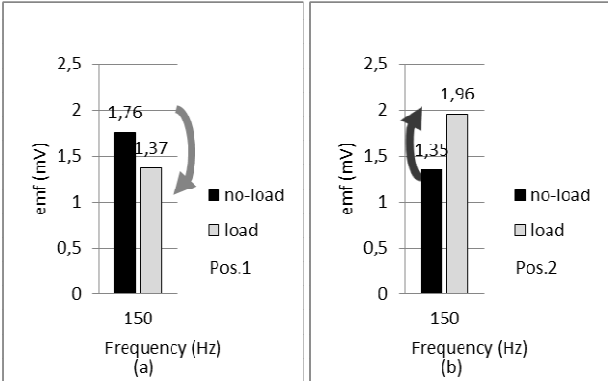


Fig. 18. Harmonic components at 150 Hz for faulty salient-pole synchronous machine (generator) at no-load and load operations

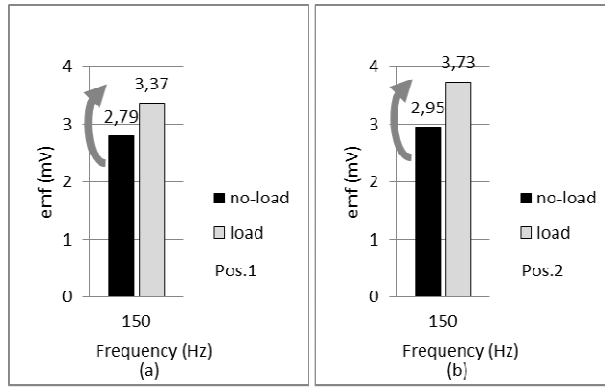


Fig. 19. Harmonic components at 150 Hz for a healthy permanent magnet synchronous motor at no-load and load operations

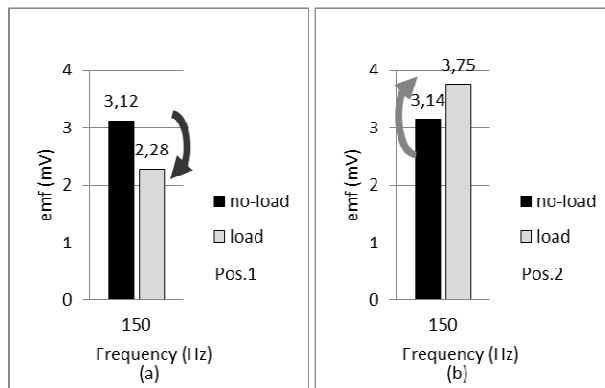


Fig. 20. Harmonic components at 150 Hz for a healthy permanent magnet synchronous motor at no-load and load operations

5.2.2 Inter-turn short circuit in induction machines

In order to generalize the proposed method, the tests have been also realized on a $p = 2$, 50Hz, 11kW, 380/660V, $N^s = 24$ and $N^r = 16$ squirrel cage induction motor (Fig. 21).

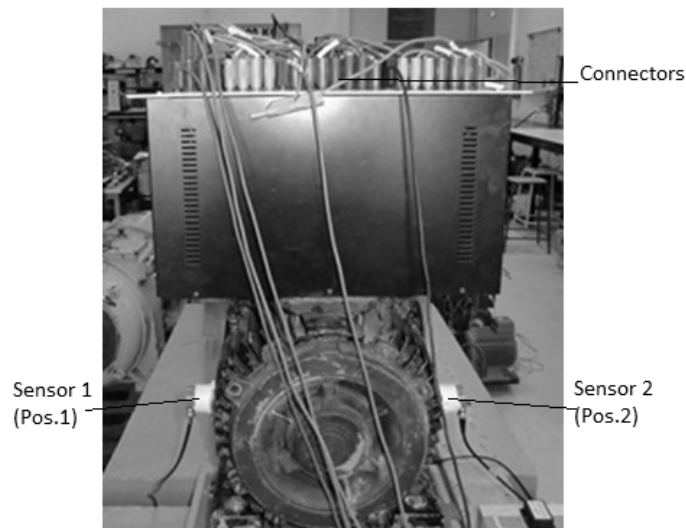


Fig. 21. Modified squirrel cage induction motor and sensors' positions

This machine, connected to the grid, has been rewound so that the terminals of the different stator elementary sections are extracted from the winding and are brought back to a connector block which is fixed above the machine. So it is possible to produce short-circuits between elementary coils. Verification have also be done in order to make sure that the currents in the wires going up from the machine towards the connector block do not disturb the measurements. Pos.1 and Pos.2 correspond respectively to β_0 and $\beta_0 + \pi$, β_0 is chosen “arbitrarily”. One will be interested to the spectral line at 850Hz ($k^r = \pm 1$). The results obtained by considering the harmonic of rank $K = K_{sc} = 17$ (850Hz at no-load and load), are presented in Figs. 22 and 23.

The phenomena are similar than that obtained in the case of synchronous machines:

- **under healthy condition** – the lines relative to $K = K_{sc} = 17$ evolve in the same way with the load (Fig. 22),
- **under faulty condition** – these lines evolve in opposite way with the load (Fig. 23).

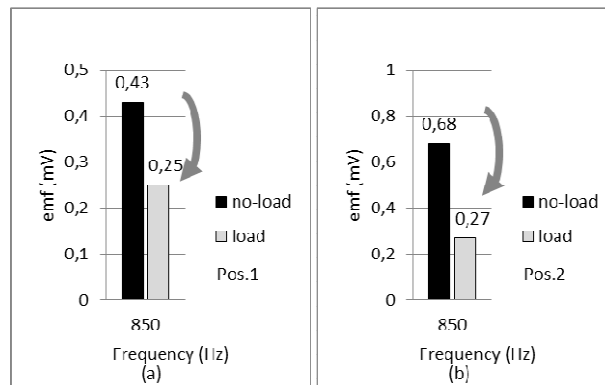


Fig. 22. Harmonic components relative to $K = K_{sc} = 17$ for healthy induction motor at no-load and load operations

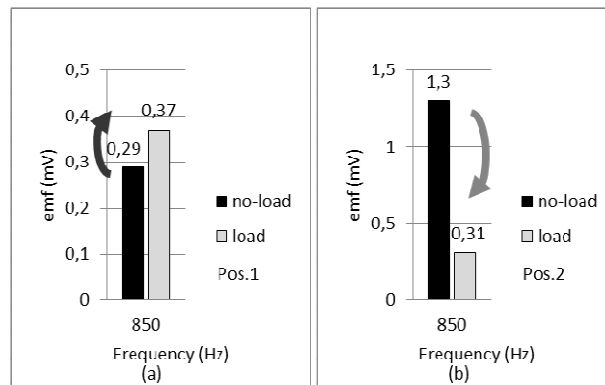


Fig. 23. Harmonic components relative to $K = K_{sc} = 17$ for faulty induction motor at no-load and load operations

This method is thus applicable to salient-pole synchronous machine, permanent magnet synchronous motor and induction motor often used in electrical traction applications and that confirm the universal quality of proposed diagnosis method.

5.3 Broken rotor bar in induction machine

The tests are performed on 4 poles, 4 kW / 50 Hz, 3×380 V squirrel cage induction motor under healthy and faulty (broken rotor bar) conditions. The obtained results at full load are shown in Figs. 24 and 25.

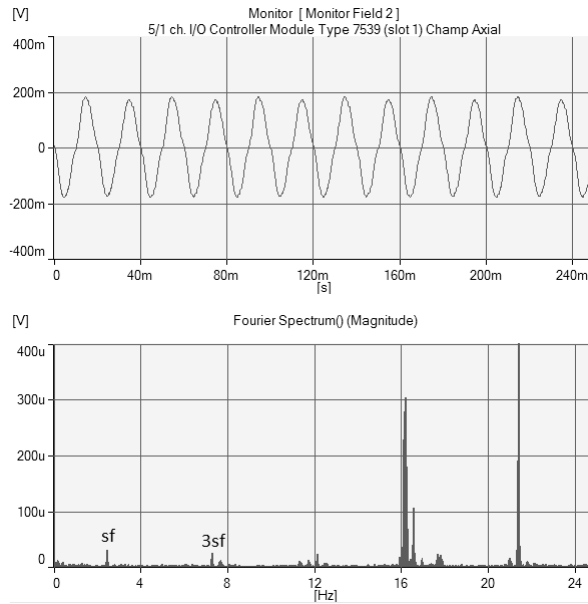


Fig. 24. Frequency spectrum of the external magnetic field (Pos.1) for healthy squirrel cage induction motor ($s = 5\%$)

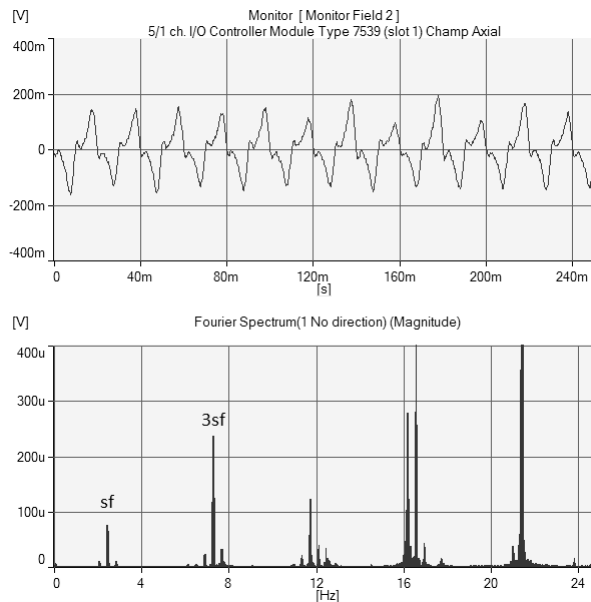


Fig. 25. Frequency spectrum of the external magnetic field (Pos.1) squirrel cage induction motor with one broken rotor bar ($s = 5\%$)

If the rotor has a broken bar, the frequency component $3sf$ is more sensitive than other components and it denotes the speed variation at frequency $2sf$, caused by a fault. Figure 25 shows that the amplitude of this harmonic is higher in comparison with the component sf (eccentricity indicator).

Also, one can observe in the case of healthy machine, the presence of frequency components sf and $3sf$ with low amplitude. It is produced because no machine can be constructed with perfect symmetry.

6. Conclusions

The paper presents a simple method to insure the supervision of AC machines used in electrical traction. This supervision can detect the stator and the rotor faults using original signatures presented in the paper. Under stator winding faults the signature concerns the harmonic at 150 Hz for synchronous machines and the slotting harmonic at 850 Hz for induction machines. This diagnosis

method does not require the knowledge of the healthy signature. It is based on comparison that concerns the state at no-load and load operations.

The indicators of rotor faults are the low frequency components of the flux spectrum at sf and $3sf$ frequencies. The diagnosis method consists in checking the magnitude of the component $3sf$ generated by the speed variation that can be compared to this of the component sf .

The advantages of proposed non invasive methods compared to other existing methods are their simplicity to implement, to interpret and a low cost set-up. The processed emf signal, delivered by a simple coil sensor, is able to indicate the presence of the fault. Moreover, the low frequency analysis is not disturbed by other sources of magnetic field presented in vicinity. Finally, the experimental tests realized on the different AC machines confirm the validation of used models and proposed methods for stator and rotor fault detection. The simulation and experimental analyses confirm the models and used approaches.

References

- [1]. R. Pusca "Contribution to the study of the driving of a mobile platform to test electrical power train components. Design of a simulator and real time system.," Doctoral thesis, Science for Engineering, Belfort, University of Franche-Compte, France, 2002.
- [2]. A. Bellini, F. Filippetti, C. Tassoni, and G. A. Capolino, "Advances in diagnostic Techniques for induction machines", *IEEE Trans. Ind. Electron.*, vol.55, no. 12, Dec. 2008; 55(12), pp. 4109-4125.
- [3]. W. T. Thomson and M. Fenger, "Current signature analysis to detect induction motor faults," *IEEE Ind. Appl. Mag.*, 2001; 7(4): 26–34.
- [4]. G. B. Kliman, R. A. Koegl, J. Stein, R. A. Koegl, R. D. Endicott, and M. W. Madden, "Noninvasive detection of broken rotor bars in operating induction motors," *IEEE Trans. Energy Convers.*, 1988; 3 (4): 873–879.
- [5]. G. B. Kliman and J. Stein, "Methods of motor current signature analysis," *Elect. Power Compon. Syst.*, 1992, 20 (5): 463–474.
- [6]. A. Khezzar, M. Y. Kaikaa, M. El Kamel Oumaamar, M. Boucherma, and H. Razik, "On the use of slot harmonics as a potential indicator of rotor bar breakage in the induction machine", *IEEE Trans. Ind. Electron.*, 2009; 56 (11): 4592-4605.
- [7]. R. Romary, R. Corton, D. Thailly, J.F. Brudny, "Induction machine fault diagnosis using an external radial flux sensor," *EPJ. Applied physics*, 2005; 32 (2): 125-132.
- [8]. F. Filippetti, G. Franceschini, C. Tassoni, and P. Vas, "AI techniques in induction machines diagnosis including the speed ripple effect," *IEEE Trans. Ind. Appl.*, 1998; 34 (1): 98–108.
- [9]. N. Arthur and J. Penman, "Induction Machine Condition Monitoring with Higher Order Spectra," *IEEE Trans. Ind. Electron.*, 2000; 47 (5):1031–1041.
- [10]. A Menacer., M.S. Nat-Said, A.H. Benakcha, and S. Drid "Stator current analysis of incipient fault into induction machine rotor bars," *Journal of Electrical Engineering* 2004; 55: 122–30.
- [11]. W.D. Li and C.K. Mechefske "Detection of induction motor faults: A comparison of stator current, vibration and acoustic methods," *Journal of Vibration and Control* 2006; 12: 165–88.
- [12]. Thailly, D.; Romary, R.; Lecointe, J.Ph.; Brudny, J.F.; Suau, P. Synchronous machine diagnosis using an external magnetic flux sensor. Presented at the *17th International Conference on Electrical Machines, ICEM 2006*; Chania, Crête, September 2006, pp. 462-468.
- [13]. A. Yazidi, H. Henao, G.A. Capolino, M. Artioli, F. Filippetti, D. Casadei, "Flux signature analysis: an alternative method for the fault diagnosis of induction machines," in *Proc. IEEE PowerTech*, St. Petersburg, Russia, 2005, pp. 1–6.
- [14]. A. Ceban, R.Pusca, R. Romary, "Eccentricity and broken rotor bars faults - Effects on the external axial field", in *Proc. ICEM Conf.*, Roma, Italy, Sep. 6-8, 2010, pp 1-6.
- [15]. P. Tavner, L. Ran, J. Penman, and H. Sedding, *Condition Monitoring of Rotating Electrical Machines*, 2nd ed. Stevenage, U.K.: IET, 2008.
- [16]. H. Henao, C. Demian, and G. A. Capolino, "A frequency-domain detection of stator winding faults in induction machines using an external flux sensor," *IEEE Transactions on Industry Applications*, vol. 39, September/October, 2003, pp. 1272-1279.
- [17]. A. Yazidi, H. Henao, G. A. Capolino, M. Artioli, F. Filippetti, and D. Casadei, "Flux signature analysis: An alternative method for the fault diagnosis of induction machines," in *2005 IEEE Russia Power Tech*, 2005; pp. 1-6.

- [18]. V. Kokko, "Condition monitoring of squirrel-cage motors by axial magnetic flux measurements," Doctoral thesis, Department of Electrical Engineering, University of Oulu, Oulu, Finland, 2003.
- [19]. M. D. Negrea, "Electromagnetic flux monitoring for detecting faults in electrical machines," Doctoral thesis, Electrical and Communications Engineering, Helsinki University of Technology, Helsinki, Finland, 2006.
- [20]. P. Werynski, "Viellissement des diélectriques et surveillance in situ des machines électriques," Thèse de doctorat, Laboratoire Systèmes Electrotechniques et Environnement (LSEE), Université d'Artois, Béthune, France, 2006.
- [21]. F. Zidat, "Conception d'une cellule de suivi des performances d'éco-efficacité énergétique des machines électriques tournantes à courant alternatif," Thèse de doctorat, Laboratoire Systèmes Electrotechniques et Environnement (LSEE), Université d'Artois, Béthune, France, 2012.
- [22]. D. Thailly, "Etude du champ de dispersion des machines à courant alternatif: Application au diagnostic," Thèse de doctorat, Laboratoire Systèmes Electrotechniques et Environnement (LSEE), Université d'Artois, Béthune, France, 2007.
- [23]. W. T. Thomson, "A review of on-line condition monitoring techniques for three-phase squirrelcage induction motors—past, present and future," in *2nd IEEE International Symposium on Diagnostics for Electrical Machines, Power Electronics and Drives - SDEMPED '99*, Gijon, Spain, (1999), 3-17.
- [24]. S. Tumanski, "Induction coil sensors - a review," *Measurement Science and Technology*, 2007; 18: 31-46.
- [25]. A. Ceban, R. Pusca, and R. Romary, "Supervision of electric traction motors by external magnetic field analysis," in *4th International Conference on Electronics, Computers and Artificial Intelligence - ECAI 2011*, Pitesti, Romania, 2011 pp. 1-10.
- [26]. R. Pusca, R. Romary, A. Ceban, and J.F. Brudny, "An online universal diagnosis procedure using two external flux sensors applied to the ac electrical rotating machines," *Sensors*. 2010; 10: 10448-10466.
- [27]. A. H. Bonnett and G. C. Soukup, "Cause and analysis of stator and rotor failures in three-phase squirrel-cage induction motors," *IEEE Transactions on Industry Applications*, 1992; 28: 921-937.
- [28]. S. Nandi, H. A. Toliyat, and L. Xiaodong, "Condition monitoring and fault diagnosis of electrical motors—a review," *IEEE Transactions on Energy Conversion*, 2005; 20: 719-729.
- [29]. D. F. Busse, J. M. Erdman, R. J. Kerkman, D. W. Schlegel, and G. L. Skibinski, "The effects of PWM voltage source inverters on the mechanical performance of rolling bearings," *IEEE Transactions on Industry Applications*, 1997; 33: 567-576.
- [30]. B. Vaseghi, "Contribution à l'étude des machines électriques en présence de défaut entre-spines," Thèse de doctorat, INPL-GREEN Université Henri Poincaré - Nancy-I, Nancy, France, 2009.
- [31]. D. G. Dorrell and A. C. Smith, "Calculation of UMP in induction motors with series or parallel winding connections," *IEEE Transactions on Energy Conversion*, 1994; 9: 304-310.
- [32]. D. G. Dorrell, W. T. Thomson, and S. Roach, "Analysis of airgap flux, current, and vibration signals as a function of the combination of static and dynamic airgap eccentricity in 3-phase induction motors," *IEEE Transactions on Industry Applications*, 1997; 33: 24-34.
- [33]. A. Ceban, R. Pusca, and R. Romary, "Study of rotor faults in induction motors using external magnetic field analysis," *IEEE Transactions on Industrial Electronics*, 2001; 593: 2082-2092.
- [34]. G. R. Bossio, C. H. De Angelo, J. M. Bossio, C. M. Pezzani, and G. O. Garcia, "Separating Broken Rotor Bars and Load Oscillations on IM Fault Diagnosis Through the Instantaneous Active and Reactive Currents," *IEEE Transactions on Industrial Electronics*, 2009; 56: 4571-4580.
- [35]. F. Filippetti, G. Franceschini, C. Tassoni, and P. Vas, "AI techniques in induction machines diagnosis including the speed ripple effect," *IEEE Trans. Ind. Appl.*, 1998; 34 (1) 98-108.
- [36]. G. Didier, H. Razik, A. Rezzoug "An induction motor model including the first space harmonics for broken rotor bar diagnosis," *Euro. Trans. Electr. Power*, 2005; 15: 229-243.
- [37]. A. Bellini, F. Filippetti, G. Franceschini, and C. Tassoni, "Quantitative evaluation of induction motor broken bars by means of electrical signature analysis," *IEEE Trans. Ind. Appl.*, 2001; 37 (5): 1248-1255.

Annexe

For a numerical application it is considered an induction machine with $p=2$, $N^s = 24$, $N^r = 16$, $R_{int}^{ts} = 0.0825$ m, $R_{ext}^{ts} = 0.121$ m and a short circuit in the phase 1. Here 12.5% of the phase coils are short-circuited and the short-circuit current is $i_{sc}^s = 3i^s$. The values that can take the coefficients that contribute to the description of predominant components are given by:

$$k^s \in (-\infty; +\infty); k^r \in (-\infty; +\infty); k'^s \in (-\infty; +\infty); k'^r \in (-\infty; +\infty);$$

$$h^s = 6k + 1; h^r \in (1, 3, 5, \dots, +\infty)$$

If we conduct the study for the first lines of rotor teeth obtained for $k^r = \pm 1$, for one healthy induction machine with a slip null and considering $k^r = -1$ we obtain:

$$k^r N^r = -16 \text{ et } K = -15, f = 750 \text{ Hz.}$$

In order to have $k^s N^s + k^r N^r$ the lowest possible (here equal to -6), we must have $k^s = 1$. Also, we find that the dominant mode is obtained for $h^s = -5$, $H = 6$ (in absolute terms and because $p = 2$). For $k^r = 1$ we obtain :

$$k^r N^r = 16 \text{ et } K = 17, f = 850 \text{ Hz.}$$

As $k^s N^s + k^r N^r$ must be the lowest possible (here equal to -2), we must have $k^s = -1$. Also, we find that the dominant mode is obtained for $h^s = 7$, $H = 2$ (in absolute terms).

The other components defined for values k^s , k^r , k'^s , k'^r , h^s , h^r of the lowest possible for the healthy machine and for the faulty coils are gives respectively in Table 1 and Table 2 with the amplitude in $x = R_{ext}^s$ gives relative to fundamental.

Table 1: Components generated by the healthy IM

k^r	k^s	h^s	K	H	$K\omega$ (Hz)	κ_{H}^{js}	$\hat{b}_{K,H}^x / \hat{b}_{11}^x$
-1	1	-5	-15	6	-750	5.09e-05	2.99e-05
-1	1	-11	-15	-6	-750	5.09e-05	8.16e-06
1	-1	7	17	-2	850	8.16e-04	2.62e-04
1	-1	13	17	10	850	3.97e-06	5.32e-07
-2	1	7	-31	-2	-1550	8.16e-04	-2.49e-04
-2	2	-17	-31	-2	-1550	8.16e-04	5.66e-05
2	-1	-5	33	6	1650	5.09e-05	-2.85e-05
2	-1	-11	33	-6	1650	5.09e-05	-7.76e-06
2	-2	13	33	-6	1650	5.09e-05	3.81e-06
2	-2	19	33	6	1650	5.09e-05	4.04e-06

Table 2: Components generated by the faulty coils

k'^r	k'^s	h	K_{cc}	H_{cc}	$K_{cc}\omega$ (Hz)	$\kappa_{H_{cc}}^{js}$	$\hat{b}_{K_{cc},H_{cc}}^x / \hat{b}_{11}^x$
-1	1	-10	-15	6	-750	5.09e-05	1.82e-05
-1	1	-13	-15	3	-750	3.76e-04	-7.31e-05
-1	1	-14	-15	2	-750	8.16e-04	-2.07e-04
-1	1	-15	-15	1	-750	0.0023	-3.78e-04
-1	1	-18	-15	-2	-750	8.16e-04	1.60e-04
-1	1	-19	-15	-3	-750	3.76e-04	4.94e-05
-1	1	-21	-15	-5	-750	9.72e-05	-1.15e-05
-1	1	-22	-15	-6	-750	5.09e-05	-8.09e-06
1	-1	10	17	-6	850	5.09e-05	1.82e-05
1	-1	11	17	-5	850	9.72e-05	2.23e-05
1	-1	14	17	-2	850	8.16e-04	-2.07e-04

1	-1	15	17	-1	850	0.0023	-3.78e-04
1	-1	17	17	1	850	0.0023	3.33e-04
1	-1	18	17	2	850	8.16e-04	1.60e-04
1	-1	21	17	5	850	9.72e-05	-1.15e-05
1	-1	22	17	6	850	5.09e-05	-8.09e-06
-2	1	17	-31	1	-1550	0.0023	-3.16e-04
-2	1	21	-31	5	-1550	9.72e-05	1.09e-05
-2	1	22	-31	6	-1550	5.09e-05	7.70e-06
-2	2	-26	-31	6	-1550	5.09e-05	3.78e-06
2	-1	-10	33	6	1650	5.09e-05	-1.73e-05
2	-1	-13	33	3	1650	3.76e-04	6.96e-05
2	-1	-14	33	2	1650	8.16e-04	1.97e-04
2	-1	-15	33	1	1650	0.0023	3.60e-04
2	-1	-18	33	-2	1650	8.16e-04	-1.52e-04
2	-2	26	33	-6	1650	5.09e-05	3.78e-06